CORE
Metadata, citation and similar papers at core.ac.uk
Provided by Loughborough University Institutional Repository

Effect of Temperature on Magnetic Solitons Induced by Spin-Transfer Torque

Sergi Lendínez,[1,*] Jinting Hang,[2] Saül Vélez,[3] Joan Manel Hernández,[1] Dirk Backes,[2,†] Andrew D. Kent,[2] and Ferran Macià[1,4,‡]

[1]*Department of Condensed Matter Physics, University of Barcelona, 08028 Barcelona, Spain*
[2]*Department of Physics, New York University, New York, New York 10003, USA*
[3]*CIC nanoGUNE, 20018 Donostia-San Sebastian, Basque Country, Spain*
[4]*Institut de Ciència de Materials de Barcelona (ICMAB-CSIC), Campus UAB, 08193 Bellaterra, Spain*

(Received 4 October 2016; revised manuscript received 12 December 2016; published 31 May 2017)

Spin-transfer torques in a nanocontact to an extended magnetic film can create spin waves that condense to form dissipative droplet solitons. Here we report an experimental study of the temperature dependence of the current and applied field thresholds for droplet soliton formation, as well as the nanocontact's electrical characteristics associated with droplet dynamics. Nucleation requires lower current densities at lower temperatures, in contrast to typical spin-transfer-torque-induced switching between static magnetic states. Magnetoresistance and electrical noise measurements (10 MHz-1 GHz) show that droplet solitons become more stable at lower temperature. These results are of fundamental interest in understanding the influence of thermal noise on droplet solitons and have implications for the design of devices using the spin-transfer-torque effects to create and control collective spin excitations.

DOI: 10.1103/PhysRevApplied.7.054027

I. INTRODUCTION

The spin-transfer-torque (STT) effect between itinerant electron spins and magnetization [1–3] is an important discovery in nanomagnetism because it provides a means of manipulating magnetization states without using magnetic fields. The angular momentum of a spin-polarized electrical current can be transferred to the magnetic moments of a magnetic material [4]. An important application of STT is magnetic random-access memory that uses the static states of bistable nanomagnets whose magnetization is oriented using spin-polarized currents [5]. The physics governing the transitions between static magnetic states under the STT effect in bistable nanomagnets, such as those incorporated in magnetic tunnel-junction pillars, are typically described through statistical mechanics [6] considering thermal fluctuations and effective energy barriers that depend on spin-polarized current. An increase in temperature leads to a faster rate of transition between magnetic states and, thus, to a reduction of their stability as well as a lower current density for STT switching [7]. The STT effect can also serve to create or modify dynamic collective excitations such as spin waves or dissipative solitons [8]. Tunable oscillators controlled by polarized currents have been proposed as building blocks for new spintronic devices [9,10]. These collective spin excitations are, in general, noisy, and their stability is more complex than magnetic static states such as those in spin valve nanopillars because in addition to the competing magnetic energies, dissipation plays a role.

Spin currents in a nanometer-scale electrical point contact to an extended ferromagnetic thin film have been used to excite linear propagating modes [11,12] and dissipative soliton modes [13–15]. Dissipative magnetic droplet solitons (droplets hereafter) are nonlinear confined wave excitations consisting of partially reversed precessing spins that can be created in films with perpendicular magnetic anisotropy (PMA) through the local suppression of the magnetic damping [16]. Droplets have been experimentally created using the STT effect in nanocontacts to PMA films [17–23], and droplets are a particular case of STT oscillators. Recently reported experiments have shown that the stability of these collective excitations is limited by the appearance of drift instabilities, which were attributed to the disorder—local variations of the effective magnetic field [21,24]. Wills *et al.* [25] identified theoretically an intrinsic deterministic linear instability and thermal fluctuations as additional instability mechanisms.

In this study, we report temperature-dependent measurements of the thresholds for droplet-soliton excitations induced by spin-polarized currents. We map the conditions in applied field and electrical current that allow droplet-soliton formation as a function of temperature. We find that lowering the temperature stabilizes the droplet states. A smaller current density is also, required to create and sustain droplet states at lower temperatures. Additionally, we observe that the temperature enhances the electrical noise associated with droplet-soliton dynamics, which correlates with a lower dc step change in nanocontact resistance when a

*Present address: Materials Science Division, Argonne National Laboratory, Lemont, IL 60439, USA.
†Present address: Department of Physics, Loughborough University, Loughborough LE11 3TU, United Kingdom.
‡fmacia@icmab.es

 © 2017 American Physical Society

droplet forms. The electrical noise and resistance are, thus, parameters that can be measured to characterize droplet stability.

II. EXPERIMENT DETAILS

The samples we study are nanocontacts (150 nm in nominal diameter) to a magnetic bilayer structure consisting of a free layer (FL) composed of cobalt (Co) and nickel (Ni) with PMA and a polarizing layer (PL) of $Ni_{80}Fe_{20}$ (permalloy) with in-plane magnetization [20] [see Fig. 1(a)]. The layer stack composition is 3Ta|50Cu|10Py|10Cu|$(0.2\text{Co}|0.6\text{Ni})\times 4|0.2\text{Co}|3\text{Pt}$ (thicknesses in nanometers) and is deposited on oxidized silicon substrates using a combination of magnetron sputtering and *e*-beam evaporation within the same ultrahigh-vacuum chamber. The FL and PL are magnetically decoupled with a 10-nm-thick copper (Cu) layer. We characterize the layers using magnetometry and ferromagnetic resonance spectroscopy [26]. The FL has an effective anisotropy field of $\mu_0 H_{\text{eff}} = \mu_0(H_K - M_s) \simeq 0.25$ T, indicating a strong PMA. The PL is a soft magnetic material with a saturation magnetization of $\mu_0 M_s \simeq 1$ T, and its magnetization lies in the plane in the absence of an applied field. We use *e*-beam lithography to define nanocontacts with diameters ranging from 70 to 200 nm in resist. We then transfer the resist pattern into a 50-nm-thick SiO_2 layer deposited on the magnetic films using reactive ion etching to create the nanocontact opening to the magnetic layer. The resist is removed, and a top electrode is deposited into the opening. The overall bottom electrode and top electrode pattern is suitable for both dc and high-frequency (up to 40 GHz) electrical measurements.

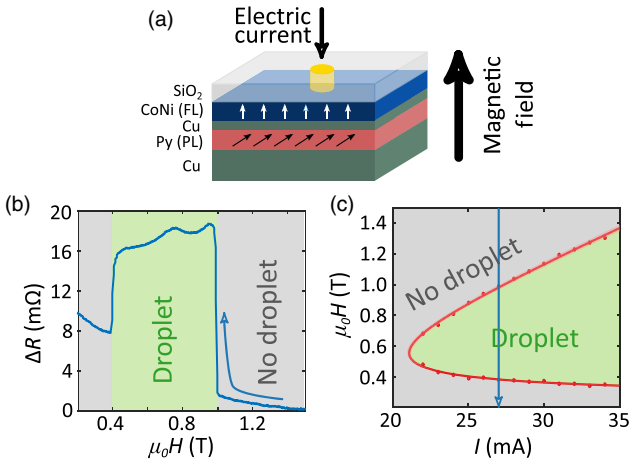

FIG. 1. (a) Schematic of the electrical point contact to a magnetic bilayer structure. An electrical current flows through a nanocontact to a thin ferromagnetic layer (free layer, FL) and a spin-polarizing layer (PL). (b) Nanocontact resistance variation as a function of the field at $T = 150$ K with a current of 27 mA showing the creation and annihilation of a droplet state. The green area represents the droplet state, whereas in the gray area, the FL magnetization is aligned with the external applied field. (c) Measured stability map for the droplet soliton as a function of magnetic field and electrical current at 150 K. The blue vertical line indicates the current at which the field sweep presented in (b) is conducted.

The electrical response of the nanocontact depends on the relative orientation of the FL's and PL's magnetization due to the giant magnetoresistance (GMR) effect. A low resistance value corresponds to the layer magnetizations being parallel (P), whereas a high value corresponds to an antiparallel (AP) alignment; the overall normalized magnetoresistance is, thus, $\bar{R}_0 = (R_{\text{AP}} - R_{\text{P}})/R_{\text{P}}$, where $R_{\text{AP,P}}$ is the resistance of the nanocontact with AP and P magnetization states. At large perpendicular applied fields, $H > M_s$, the PL magnetization is saturated in the field direction, resulting in a P state with a minimum value for the resistance of the nanocontact. When a droplet state forms in the FL, the magnetization (partially) reverses, and an increase of the resistance is expected. The resistance change will be the largest, $\bar{R}_0$, when the spins in the droplet are completely reversed and the droplet fully occupies the nanocontact region. At small applied fields $H < M_S$, the PL magnetization has only a component in the direction of the FL magnetization, which results in a linear decrease of the nanocontact resistance with the applied field; droplet formation will still produce a change in resistance, this time, proportional to the magnetization component of the PL in the perpendicular direction. Precession of the in-plane component of the FL magnetization results in an oscillating resistance and consequently a voltage response in the microwave range. We note that this voltage signal appears only for fields lower than the saturation field $\simeq 1$ T of the PL (i.e., when the polarizing layer has a component of magnetization in the film plane) and vanishes when the PL is saturated in the same direction as the FL magnetization. Representative high-frequency noise spectra versus dc current of our samples at room temperature are shown in Appendix A. A low-frequency signal with a characteristic time scale of hundreds of megahertz has been recently measured [21,23] in droplet states and has been associated with center-of-mass droplet motion, such as the droplet drifting outside the nanocontact region.

In Fig. 1(b), we plot a measured magnetoresistance curve [17,19,20] at a fixed current of 27 mA ramping the perpendicular applied field from high to low field at a fixed temperature of 150 K. This shows first the creation (at 1 T) and then the annihilation of the droplet state (0.4 T). Figure 1(c) shows a measured droplet stability map in magnetic field and current space [21,23] built from magnetoresistance curves measured at different applied current at a fixed temperature of 150 K. The no droplet state is plotted in gray and corresponds to a lower resistance state, whereas the green area represents the droplet state, a higher resistance state.

In order to study the temperature dependence of the dc and ac resistance, we wire bond our nanocontact to sample

holders capable of transmitting microwave signals up to 4 GHz and introduce them into a cryostat that allows variations of temperature from 2 to 350 K and bipolar fields up to 9 T. We are able to vary the angle between the film plane and the applied field by rotating the sample holder. We use a current source and a voltmeter to measure the dc-resistance response and a spectrum analyzer to study the spectral composition of the electrical noise of the nanocontact. A bias tee separates the dc and ac components of the signal. The resistance measurements allow us to determine the relative orientation of the magnetization between the FL and PL via the GMR effect. The experimental results shown in the following are done with a magnetic field applied perpendicular to the film plane. We note that the droplet states can be affected by Joule heating [7], especially the FL precession [27,28]. We, thus, obtain our data by always keeping the electrical current constant and sweeping the magnetic fields.

III. RESULTS AND DISCUSSION

We first study the creation and annihilation of the droplet through dc measurements of the magnetoresistance. Figure 1(b) shows the data at $T = 150$ K with decreasing applied magnetic field (the field is swept from −3 to 3 T and back). At zero applied field, the PL and FL are orthogonal, and current through the nanocontact that is polarized in the direction of the PL creates a torque that averages to zero over one precessional cycle. As the magnetic field increases, the PL magnetization tilts and increases the electrical current's spin polarization in the direction of the FL magnetization; eventually, the STT effect on the FL compensates the damping and allows for the nucleation of a droplet. Larger fields ultimately destabilize and annihilate the droplet, favoring an alignment of the two layers' magnetization in the direction of the applied field. As we sweep the field down back to zero, the droplet nucleates and annihilates at similar field values as in the sweep up, showing hysteresis in some cases [17,20], which indicates stability of the droplet states (see Appendix B for a sample with pronounced hysteresis).

We measure the stability maps of the droplet as a function of temperature. Figure 2 shows the field and current values that allow for droplet-state formation at different temperatures (from 50 to 250 K). We observe how the region of droplet stability increases as the temperature is lowered, indicating that smaller current densities are needed to create and sustain droplets at lower temperatures. The measurements of a different sample are presented in Appendix B in the range of 2 to 350 K.

The boundaries determining the region of droplet existence present a minimum current at a particular value of applied field (below that current value, the droplet cannot be generated regardless of the field). An analytic prediction for the variation of the onset current as a function of the applied field is not available because of the sample's

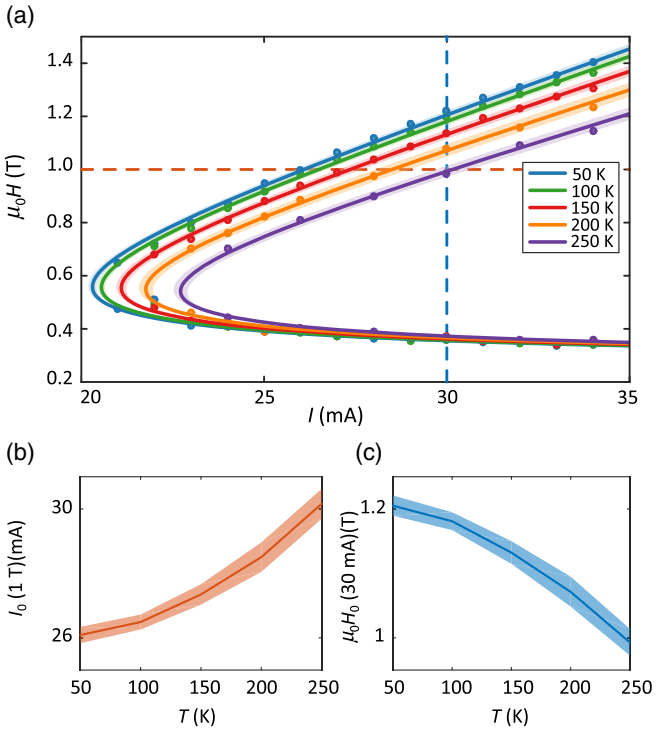

FIG. 2. (a) Stability maps of soliton states as a function of temperature (50 to 250 K). The points show the current and field combination at which the droplet is created. The curves are fits to the data. (b), (c) Temperature dependence of the onset current at a fixed magnetic field of 1 T (b) and of the onset field at a fixed current of 30 mA (c) obtained from the fits. The light colors in the graphs show the uncertainties.

orthogonal geometry (i.e., the PL perpendicular to the FL in zero applied field). Hoefer *et al.* [16] provided an expression for the minimum sustaining current in the case of having a PL always magnetized normal to the film plane that was proportional to the damping parameter and to the precessing frequency—that is also proportional to the applied field. However, in our samples, we need an applied field larger than approximately 1 T to ensure the PL magnetization is normal to the film plane. At fields that do not completely align the magnetization of the two layers, the degree of spin polarization of the electrical current in the direction of the FL plays an important role. The polarization degree depends on the magnetization component of the PL normal to the film plane, and the magnetization is proportional to the applied field. Thus, the onset current has an inverse dependence with the applied magnetic field at low fields, as reported in several experimental studies [19,20,23,29]. Chung *et al.* [23] recently used an expression for the onset current as a function of the field that accounts for the effect of a PL that is not aligned with the FL. Their approximation for the onset current as a function of the applied field summarizes the previous discussion; its derivation is based on the Slonczewski critical current condition [30] in a material with PMA

and consists of a term proportional to the applied field that dominates at large fields and another that is inversely proportional to the same field that dominates at lower field values,

$$I_c = a\mu_0 H + \frac{b}{\mu_0 H} + c. \quad (1)$$

Our data fit poorly to such expression (see Appendix C), but instead they fit well when we consider a shifted value for the applied field, $H \to (H - H')$, with $\mu_0 H' \simeq 0.27$ T, which matches with the anisotropy field of the FL. Figure 2(a) shows the fits to the data (see Appendix C for plots of fitting parameters, a, b, c, and $d = \mu_0 H'$, as a function of temperature).

We observe that smaller currents are required to create droplet solitons at lower temperatures. As a result, there is also an increase in the maximum field at which droplet states occur. We plot these two indicative quantities in Figs. 2(b) and 2(c); the onset current with a fixed field of 1 T and the onset field (sweeping down from large fields) at a fixed current of 30 mA. Notice that the changes become more pronounced as the temperature increases and seem to saturate when it decreases.

We characterize the overall change in resistance between the P and AP states at each temperature using magnetotransport measurements at small applied currents. The sample resistance varies with the temperature and the total MR changes as well. Figure 3(a) shows the normalized MR curves measured at different temperatures when the magnetic field is swept up from zero to 1.6 T. The overall resistance changes at each temperature $\bar{R}_0(T)$ are plotted in the inset of Fig. 3(a). The green curve in Fig. 3(a), for instance, shows a MR curve measured at 32 mA and 150 K; we can see a step increase in resistance at 0.3 T corresponding to the creation of the droplet and a second step (decrease) at 1.18 T corresponding to the droplet annihilation. At temperatures above 150 K, the MR curves show an intermediate state between the first step decrease at 1.2 T and a second step decrease at 1.5 T that indicates the presence of a partially reversed magnetization state in the nanocontact.

The MR curve measured at 150 K is plotted in Fig. 3(b) along with curves measured at other applied currents but at the same temperature, and we see that the onset and annihilation fields vary as in Fig. 2. We observe that within the high-resistance states (droplet states), the resistance fluctuates with the applied field indicating different droplet configurations [20] that are reproducible at different applied currents [see Fig. 3(b) for fields between 0.4 and 0.8 T]. However, when varying the temperature, we also observe, in addition to the resistance fluctuations, a decrease in the overall resistance change with increasing temperature. We, thus, confirm that the increase in temperature reduces the effective amount of reversed magnetization either because the droplet state becomes smaller than the nanocontact or because on average it spends less time in the contact region, such as due to drift instabilities [21,25]. In Appendix C, the evaluation and the analysis of the overall change in the MR in different devices with the same layer stack is shown.

In order to investigate the effect of the temperature on the droplet dynamics, we measure the electrical noise at frequencies below 4 GHz with a spectrum analyzer at the same time we measure the dc resistance. We associate the electrical noise signal with motion of the droplet soliton beneath the nanocontact; the low-frequency noise signal is present when a droplet state forms [21,23]. The electrical noise signal is mostly a $1/f$ type [see Fig. 3(d)], but in some cases, it is accompanied by a

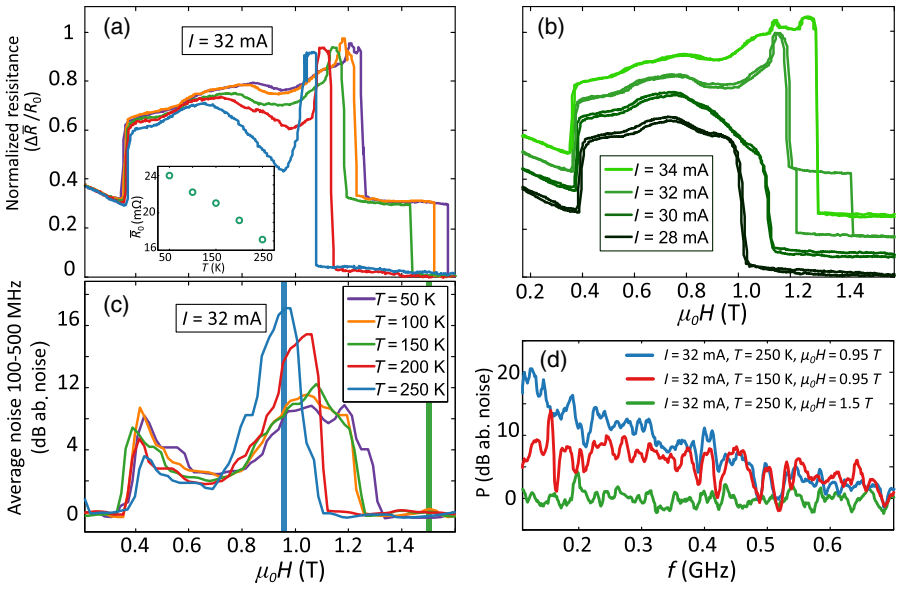

FIG. 3. (a) Normalized magnetoresistance as the field sweeps up at a fixed current of $I = 32$ mA for temperatures ranging from 50 to 250 K. The inset shows the normalizing values, $\bar{R}_0$. (b) Normalized magnetoresistance curves for both sweeps up and down at a fixed temperature $T = 150$ K for different applied currents ranging from 28 to 34 mA. (c) Low-frequency signal above noise averaged in the range 100–500 MHz measured at the same time as the magnetoresistance curve in (a). Vertical bars indicate the magnetic fields at which spectra correspond in (c). (d) Low-frequency response measured at $I = 32$ mA and $T = 250$ K at 1.5 T (green curve) and at 0.9 T (blue curve), and $T = 150$ K at 0.9 T (red curve).

resonant peak at frequencies of the order of hundreds of megahertz [21].

We observe the appearance of a low-frequency signal (electrical noise) when the sample is in a droplet state. Figures 3(a) and 3(c) show simultaneous measurements of the dc resistance and the low-frequency spectral signal, which is averaged between 100 and 500 MHz at each magnetic field [see Fig. 3(d) for frequency sweeps at a given field]. We can compare the MR curves at a fixed current of 32 mA and the corresponding low-frequency signal at five different temperatures. At 250 K, we observe that when the droplet develops at 0.35 T, there is an increase in the dc resistance and a peak in the low-frequency signal. As the field is swept up, the droplet state stabilizes, and we observe a decrease in the low-frequency signal (field values between 0.5 and 0.8 T). As we continue with the field sweep, the dc resistance slightly decreases, and the spectral signal increases indicating additional dynamics in the droplet state. A further increase of the applied field eventually annihilates the droplet state. We note that the small changes in the low-frequency signal within the droplet state as a function of the applied field shown in Fig. 3(c) are reproducible every time we sweep the field. We also observe in Figs. 3(a) and 3(c) that as the temperature is lowered, the droplet states show a larger dc signal and a decrease in spectral noise indicating a higher stability; such an effect is clearly seen at applied fields around 1 T.

We, thus, observe an evolution of droplet states, both in dc resistance and in the electrical noise, as we sweep the field. There is a correlation between the power level of the low-frequency signal and the dc-resistance signal at different temperatures; droplet states giving a large dc resistance generally produce a smaller low-frequency spectral signal. We note that the onset of droplet solitons at low fields is always associated with high levels of electrical noise and that droplet states that present only fractional variations of the dc resistance, for instance, the MR curves in Fig. 3(a) for 50, 100, or 150 K above 1.2 T, do not present measurable electrical noise, suggesting the corresponding states have little or no droplet motion. We note here that we observe variations in the electrical noise level—and, consequently, in the value of the dc signal—from sample to sample, which points toward the importance of defects and inhomogeneities in the nanocontact.

IV. CONCLUSION

Our results show that thermal fluctuations have a significant effect on the dynamics of STT-induced droplet solitons and demonstrate that the temperature can be a means of controlling droplet instabilities and droplet dynamics. Thermal effects must, thus, be considered in applications of such solitons. A first consideration is that lowering the temperature improves the stability and lowers the required energy to create and sustain droplet solitons. Another consideration is for those cases where less stable states are wanted; for instance, Maiden *et al.* [31] described how to use magnetic droplet solitons to communicate or transmit information, which requires moving droplet solitons. The same concept might apply to STT-induced dynamical Skyrmions [23]. The temperature effects also have to be taken into account for applications based on STT oscillators that exploit the high nonlinearity and their stochasticity—such as synchronizing STT oscillators through noise [32,33]. As an example, STT oscillators have been proposed as key elements in neuromorphic computation [33], and recently an experimental study has shown how to build a device that performs spoken-digit pattern recognition [34]. In sum, applications involving magnetic droplet solitons will require a detailed understanding of their noise-induced dynamics.

ACKNOWLEDGMENTS

We acknowledge technical support from Luis Hueso and Fèlix Casanova at CIC nanoGUNE. F. M. acknowledges financial support from the Ramón y Cajal program through Grant No. RYC-2014-16515 and from MINECO through the Severo Ochoa Program for Centers of Excellence in R&D (Grant No. SEV-2015-0496). The work at CIC nanoGUNE was supported by the EU 7th FP under Grant No. ERC 257654-SPINTROS and by the Spanish MINECO through Grant No. MAT2015-65159-R. Research at UB is partially supported through project MAT2015-69144-P (MINECO/FEDER, UE). Research at NYU is supported by Grant No. NSF-DMR-1610416.

APPENDIX A: HIGH-FREQUENCY CHARACTERIZATION

The samples we use in this experiment have the layer stack described in Ref. [26] and are fabricated using the same nanofabrication process as the ones published in Ref. [21], where high-frequency data were presented and discussed. Here we present data on the studied samples (150-nm-diameter electrical contacts) measured at room temperature with high-frequency (ground-signal-ground) probes (Picoprobe® from GGB Industries).

Figure 4 shows high-frequency spectra at a fixed applied current of $I = 30$ mA at different values of the applied field. Two insets plot a map of high-frequency spectra measured at fixed values of the applied field. We observe that as the current increases, the frequency increases (there is a blueshift). In some cases, we can see multiple peaks indicating that different droplet states occur. We note that with increasing applied field, the microwave signal vanishes because the magnetization of the polarizing layer saturates ($\simeq 1$ T) perpendicular to the film plane in the same direction as the free layer.

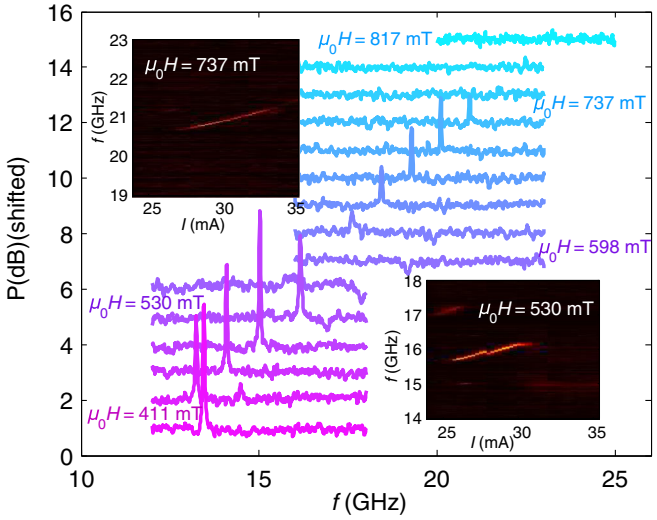

FIG. 4. High-frequency spectra: Spectra at a fixed $I = 30$ mA for different applied fields are plotted and shifted vertically for clarity. Insets represent high-frequency spectra maps at a fixed value of applied field, $\mu_0 H = 530$ and 737 mT.

APPENDIX B: DATA ON DIFFERENT SAMPLES

Here we present data on a different sample fabricated on the same layer stack with an identical geometry. The sample is measured in a larger temperature range, although we do not measure the low-frequency signal (and this is the reason why these data are not presented in the main manuscript).

Figure 5 shows the MR curves at different temperatures at a fixed current of 35 mA. As the field is swept up from 0, the droplet nucleates at small field values; when the field is further increased, the STT effect is no longer able to overcome the dissipation at higher applied field and the droplet annihilates. Sweeping the field back to zero creates the droplet state at lower field values compared with the annihilation of the sweep up, showing hysteresis, and in continuing to lower fields, it annihilates as the STT effect is too small to sustain the droplet state. For the sake of simplicity, our analysis is only of the annihilation of the droplet when sweeping the field up and creation when sweeping it down, i.e., in the high-field range, and we refer to the value of these fields as annihilation and creation fields, respectively. In the following, we report only the case of one polarity of the applied field, as the results with the other polarity are analogous.

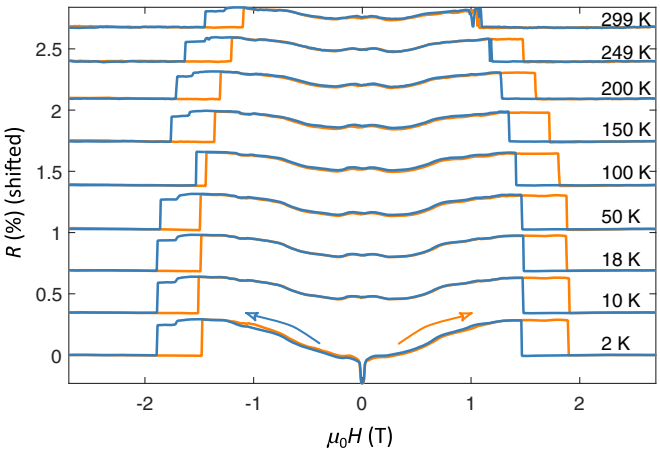

FIG. 5. MR measurements as the field is swept up from −3 to 3 T (orange) and down from 3 to −3 T (blue), for different temperatures in the range 2–300 K, at $I = 35$ mA, showing the creation and annihilation fields as the droplet is formed.

A stability diagram with measurements in the temperature range from 2 to 300 K is shown in Fig. 6(a). The curves separate the droplet state (at lower fields and larger currents) from the nondroplet state (at large fields and low currents). Colors from dark blue corresponding to 2 K to dark red corresponding to 300 K indicate the temperature at which the sample is measured. We plot only the creation points when sweeping the field from a large value down to zero because the values of the annihilation fields (when

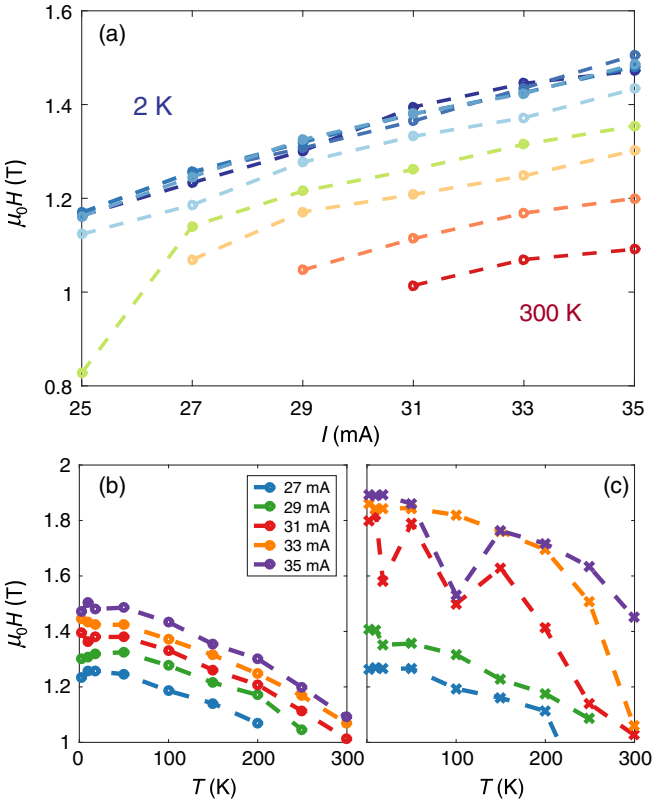

FIG. 6. (a) Stability map of soliton states as a function of temperature (50 to 300 K). There are no fits here, and the presented data are all experimental. Colors from dark blue 2 K to dark red 300 K indicate the temperatures at which the sample is measured (2, 10, 18, 50, 100, 150, 200, 250, and 300 K). We plot only the creation points when sweeping the field down. (b) shows the same data as in (a) but plotted as a function of T for different applied currents, and (c) is the same plot for the annihilation fields that are equal or larger, when there is hysteresis.

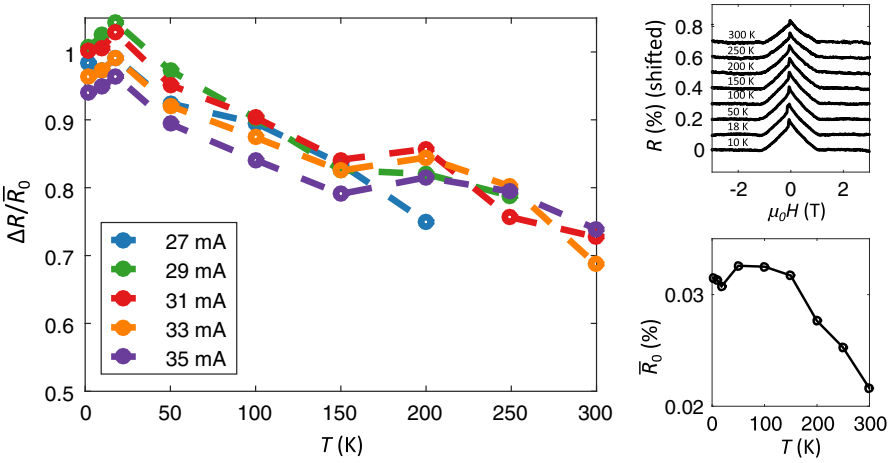

FIG. 7. (Left-hand-side panel) Normalized height of the jump $\Delta R/(\bar{R})_0$ as a function of the temperature for current values of 27 mA (blue), 29 mA (green), 31 mA (red), 33 mA (orange), and 35 mA (purple). (Top right-hand-side panel) MR measurements as the magnetic field is swept down from 3 to −3 T for different temperatures in the range 2–300 K using an applied current of $I = -2$ mA. (Bottom right-hand-side panel) Evolution of the overall change in magnetoresistance with temperature $\bar{R}_0$.

sweeping from 0 to a large field value) have a broader distribution, and, thus, the line separating one state from the other is not well defined. We also omit the onset and annihilation at lower fields caused by the loss of polarization in the current. Figure 6 shows the field values at fixed currents for both the onset [Fig. 6(b)] of droplet states (the same used to create the main stability diagram) and the annihilation [Fig. 6(c)]. We notice here that Fig. 6(c) shows that the values for annihilation have an uncertainty that is not visible in the values corresponding to the onset, indicating that the onset and annihilation might have a different origin.

In order to evaluate the change in the characteristic resistance associated to the droplet state at different temperatures, we must consider the intrinsic change in MR as a function of temperature. Thus, we measure the MR curves at a current value of −2 mA. The sign of the current is chosen to avoid excitations in the FL; i.e., it favors damping and stabilizes the FL magnetization. Moreover, a small value of 2 mA minimizes the STT, yet allowing for a measurement of the resistance. The top right-hand-side panel of Fig. 7 shows the measured MR curves at different temperatures. The step at small negative values visible in the MR curves is associated with the reversal of the FL in the direction of the external field, corresponding to the anisotropy field (the curves are measured by decreasing the magnetic field). From the MR curves, we calculate the MR value at each temperature as the overall variation of resistance normalized by the resistance value. The MR values at each temperature are plotted in the lower right-hand-side panel of Fig. 7.

The variations in resistance coming from the change in the droplet state are, thus, normalized by the intrinsic MR value at that particular field value in order to remove any temperature dependence of the MR. The left-hand-side panel of Fig. 7 shows the temperature dependence of the normalized variation in resistance. A value of 1 means that the FL and PL magnetizations are antiparallel. As the temperature increases, the reversal decreases from almost full reversal at 10–50 K to approximately 70% at room temperature.

APPENDIX C: CURVE FITTING

The expression suggested by Chung *et al.* [23] for the onset current of the droplet soliton that accounts for the effect of a PL not aligned with the FL does not fit our data. Figure 8 shows the fitting of the data presented in the main manuscript using the expression

$$I = ah + \frac{b}{h} + c, \tag{C1}$$

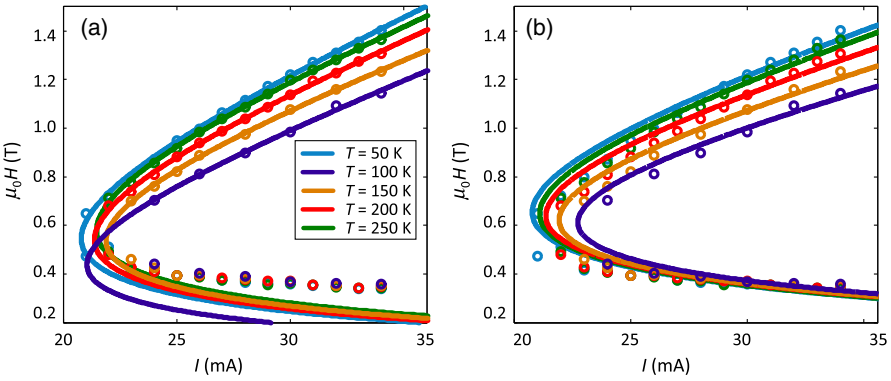

FIG. 8. Fits to the stability maps of soliton states as a function of temperature (50 to 250 K). The points show the measured data. The curves are fits to the data. The fit in (a) uses all the data points, whereas the fit in (b) uses only the points that represent the onset of a droplet soliton when sweeping the field from high to low values ($\mu_0 H > 0.6$ T)

TABLE I. Evolution of four free parameters.

T (K)	a (mA/T)	b (mA T)	c (mA)	d (T)
50	21 ± 3	2.0 ± 0.9	7 ± 5	0.25 ± 0.03
100	21 ± 4	1.8 ± 0.8	8 ± 5	0.26 ± 0.03
150	24 ± 5	2.2 ± 1.3	7 ± 7	0.26 ± 0.04
200	24 ± 7	1.7 ± 1.5	9 ± 9	0.28 ± 0.05
250	26 ± 9	1.7 ± 1.8	10 ± 11	0.28 ± 0.6

where a, b, and c are the fitting parameters. We present two fittings considering either all the points [in Fig. 8(a)] or only the points that represent the onset of a droplet soliton when sweeping the field from high to low values ($\mu_0 H > 0.6$ T). The fits are poor and cannot capture the behavior of both large and small fields.

We can fit the data by considering a shift in the applied field, $h - d$ instead of h, of approximately 0.27 T. Next, we analyze the evolution of the fitting parameters in the equation

$$I = a(h - d) + \frac{b}{h - d} + c, \tag{C2}$$

as a function of temperature.

We first consider all four parameters as free parameters. The values are summarized in Table I, and the same data are plotted in Fig. 9.

We observe that parameter b is almost constant (this parameter matters only at low fields), and parameter c has also a small variation in temperature. Thus, we fix $b = 1.9$ mA T and $c = 1.7$ mA. The parameters are again summarized in Table II, and the same data are plotted in Fig. 10.

We observe that parameter a, which indicates the slope of the line of the onset current (should be proportional to dissipation), increases considerably from 22 ma/T to almost 30 mA/T. Additionally, parameter d that matters mostly at low fields, also increases about 10% in temperature.

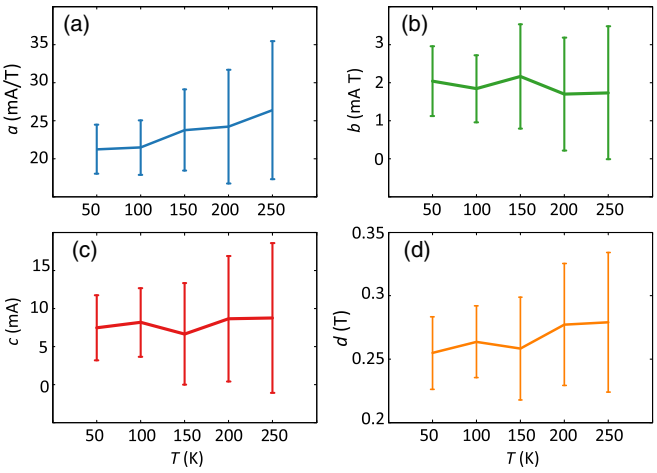

FIG. 9. Temperature evolution of free parameters used in Eq. (C2).

TABLE II. Evolution of parameters, fixing $b = 1.9$ mA T and $c = 7$ mA.

T (K)	a (mA/T)	d (T)
50	22 ± 0.08	0.264 ± 0.004
100	23 ± 0.07	0.266 ± 0.003
150	24 ± 0.09	0.271 ± 0.004
200	26 ± 0.13	0.274 ± 0.005
250	29 ± 0.14	0.278 ± 0.005

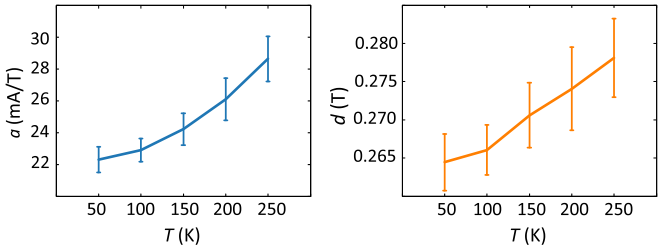

FIG. 10. Evolution of parameters, fixing $b = 1.9$ mA T and $c = 7$ mA.

[1] J. C. Slonczewski, Current-driven excitation of magnetic multilayers, J. Magn. Magn. Mater. **159**, L1 (1996).
[2] L. Berger, Emission of spin waves by a magnetic multilayer traversed by a current, Phys. Rev. B **54**, 9353 (1996).
[3] J. A. Katine, F. J. Albert, R. A. Buhrman, E. B. Myers, and D. C. Ralph, Current-Driven Magnetization Reversal and Spin-Wave Excitations in Co/Cu/Co Pillars, Phys. Rev. Lett. **84**, 3149 (2000).
[4] D. C. Ralph and M. D. Stiles, Spin transfer torques, J. Magn. Magn. Mater. **320**, 1190 (2008).
[5] Andrew D. Kent and Daniel C. Worledge, A new spin on magnetic memories, Nat. Nanotechnol. **10**, 187 (2015).
[6] William T. Coffey and Yuri P. Kalmykov, Thermal fluctuations of magnetic nanoparticles: Fifty years after Brown, J. Appl. Phys. **112**, 121301 (2012).
[7] S. Petit-Watelot, R. M. Otxoa, M. Manfrini, W. Van Roy, L. Lagae, J.-V. Kim, and T. Devolder, Understanding Nanoscale Temperature Gradients in Magnetic Nanocontacts, Phys. Rev. Lett. **109**, 267205 (2012).
[8] Arne Brataas, Andrew D. Kent, and Hideo Ohno, Current-induced torques in magnetic materials, Nat. Mater. **11**, 372 (2012).
[9] Ferran Macià, Andrew D. Kent, and Frank C. Hoppensteadt, Spin-wave interference patterns created by spin-torque nano-oscillators for memory and computation, Nanotechnology **22**, 095301 (2011).
[10] N. Locatelli, V. Cros, and J. Grollier, Spin-torque building blocks, Nat. Mater. **13**, 11 (2014).
[11] Vladislav E. Demidov, Sergei Urazhdin, and Sergej O. Demokritov, Direct observation and mapping of spin waves emitted by spin-torque nano-oscillators, Nat. Mater. **9**, 984 (2010).

[12] M. Madami, S. Bonetti, G. Consolo, S. Tacchi, G. Carlotti, G. Gubbiotti, F. B. Mancoff, M. A. Yar, and J. Akerman, Direct observation of a propagating spin wave induced by spin-transfer torque, Nat. Nanotechnol. **6**, 635 (2011).

[13] Vladislav E. Demidov, Sergei Urazhdin, and Sergej O. Demokritov, Magnetic nano-oscillator driven by pure spin current, Nat. Mater. **11**, 1028 (2012).

[14] D. Backes, F. Macià, S. Bonetti, R. Kukreja, H. Ohldag, and A. D. Kent, Direct Observation of a Localized Magnetic Soliton in a Spin-Transfer Nanocontact, Phys. Rev. Lett. **115**, 127205 (2015).

[15] S. Bonetti, R. Kukreja, Z. Chen, F. Macià, J. M. Hernàndez, A. Eklund, D. Backes, J. Frisch, J. Katine, G. Malm, S. Urazhdin, A. D. Kent, J. Stöhr, H. Ohldag, and H. A. Dürr, Direct observation and imaging of a spin-wave soliton with *p*-like symmetry, Nat. Commun. **6**, 8889 (2015).

[16] M. A. Hoefer, T. J. Silva, and Mark W. Keller, Theory for a dissipative droplet soliton excited by a spin torque nano-contact, Phys. Rev. B **82**, 054432 (2010).

[17] S. M. Mohseni, S. R. Sani, J. Persson, T. N. Anh. Nguyen, S. Chung, Ye. Pogoryelov, P. K. Muduli, E. Iacocca, A. Eklund, R. K. Dumas, Stefano Bonetti, A. Deac, M. A. Hoefer, and J. Åkerman, Spin torque-generated magnetic droplet solitons, Science **339**, 1295 (2013).

[18] S. Chung, S. M. Mohseni, S. R. Sani, E. Iacocca, R. K. Dumas, T. N. Anh Nguyen, Ye. Pogoryelov, P. K. Muduli, A. Eklund, M. Hoefer, and J. Åkerman, Spin transfer torque generated magnetic droplet solitons (invited), J. Appl. Phys. **115**, 172612 (2014).

[19] S. M. Mohseni, S. R. Sani, J. Persson, T. N. Anh Nguyen, S. Chung, Ye. Pogoryelov, P. K. Muduli, E. Iacocca, R. K. Dumas, A. Eklund, M. Hoefer, and Johan Åkerman, Magnetic droplet solitons in orthogonal nano-contact spin torque oscillators, Physica B (Amsterdam) **435**, 84 (2014).

[20] Ferran Macià, Dirk Backes, and Andrew D. Kent, Stable magnetic droplet solitons in spin-transfer nanocontacts, Nat. Nanotechnol. **9**, 992 (2014).

[21] S. Lendínez, N. Statuto, D. Backes, A. D. Kent, and F. Macià, Observation of droplet soliton drift resonances in a spin-transfer-torque nanocontact to a ferromagnetic thin film, Phys. Rev. B **92**, 174426 (2015).

[22] S. Chung, S. M. Mohseni, A. Eklund, P. Dürrenfeld, M. Ranjbar, S. R. Sani, T. N. Anh Nguyen, R. K. Dumas, and J. Åkerman, Magnetic droplet solitons in orthogonal spin valves, Low Temp. Phys. **41**, 833 (2015).

[23] Sunjae Chung, Anders Eklund, Ezio Iacocca, Seyed Majid Mohseni, Sohrab R. Sani, Lake Bookman, Mark A. Hoefer, Randy K. Dumas, and Johan Äkerman, Magnetic droplet nucleation boundary in orthogonal spin-torque nano-oscillators, Nat. Commun. **7**, 11209 (2016).

[24] L. D. Bookman and M. A. Hoefer, Perturbation theory for propagating magnetic droplet solitons, Proc. R. Soc. A **471**, 20150042 (2015).

[25] P. Wills, E. Iacocca, and M. A. Hoefer, Deterministic drift instability and stochastic thermal perturbations of magnetic dissipative droplet solitons, Phys. Rev. B **93**, 144408 (2016).

[26] Ferran Macià, P. Warnicke, D. Bedau, M.-Y. Im, P. Fischer, D. A. Arena, and A. D. Kent, Perpendicular magnetic anisotropy in ultrathin Co-Ni multilayer films studied with ferromagnetic resonance and magnetic x-ray microspectroscopy, J. Magn. Magn. Mater. **324**, 3629 (2012).

[27] Koji Sekiguchi, Keisuke Yamada, Soo-Man Seo, Kyung-Jin Lee, Daichi Chiba, Kensuke Kobayashi, and Teruo Ono, Time-Domain Measurement of Current-Induced Spin Wave Dynamics, Phys. Rev. Lett. **108**, 017203 (2012).

[28] Vincent Vlaminck and Matthieu Bailleul, Current-induced spin-wave doppler shift, Science **322**, 410 (2008).

[29] B. Oezyilmaz, A. D. Kent, D. Monsma, J. Z. Sun, M. J. Rooks, and R. H. Koch, Current-Induced Magnetization Reversal in High Magnetic Fields in Co/Cu/Co Nanopillars, Phys. Rev. Lett. **91**, 067203 (2003).

[30] J. C. Slonczewski, Excitation of spin waves by an electric current, J. Magn. Magn. Mater. **195**, L261 (1999).

[31] M. D. Maiden, L. D. Bookman, and M. A. Hoefer, Attraction, merger, reflection, and annihilation in magnetic droplet soliton scattering, Phys. Rev. B **89**, 180409 (2014).

[32] A. Mizrahi, N. Locatelli, J. Grollier, and D. Querlioz, Synchronization of electrically coupled stochastic magnetic oscillators induced by thermal and electrical noise, Phys. Rev. B **94**, 054419 (2016).

[33] A. Mizrahi, N. Locatelli, R. Matsumoto, A. Fukushima, H. Kubota, S. Yuasa, V. Cros, J. V. Kim, J. Grollier, and D. Querlioz, Magnetic stochastic oscillators: Noise-induced synchronization to underthreshold excitation and comprehensive compact model, IEEE Trans. Magn. **51**, 1 (2015).

[34] Jacob Torrejon, Mathieu Riou, Flavio Abreu Araujo, Sumito Tsunegi, Guru Khalsa, Damien Querlioz, Paolo Bortolotti, Vincent Cros, Akio Fukushima, Hitoshi Kubota, Shinji Yuasa, Mark D. Stiles, and Julie Grollier, Neuromorphic computing with nanoscale spintronic oscillators, arXiv:1701.07715.